IEEE Open Journal of
Intelligent Transportation
Systems

Received 20 August 2021; revised 21 October 2021 and 8 December 2021; accepted 10 January 2022. Date of publication 14 January 2022;
date of current version 28 January 2022.

Digital Object Identifier 10.1109/OJITS.2022.3143168

Super-Twisting Hybrid Control for Ship-Borne PMSM

DI-FEN SHI[1], RUN-MIN HOU[1], YUAN GAO[2], XIAO-HUI GU[1], AND YUAN-LONG HOU[1]

[1]School of Mechanical Engineering, Nanjing University of Science and Technology, Nanjing 210094, China

[2]Faculty of Engineering, University of Bristol, Bristol BS8 1QU, U.K.

CORRESPONDING AUTHORS: R.-M. HOU AND Y. GAO (e-mail: 187189579@qq.com; yuan21.gao@bristol.ac.uk)

This work was supported by the National Natural Science Foundation of China under Grant 51805264.

ABSTRACT In the field of ship-borne PMSM, there exists the sea wave fluctuations, external disturbances thus model uncertainties are always challenging the control design of ship-borne permanent magnet synchronous motors (PMSMs). To deal with this problem, a super-twisting extended state observer (SESO) is used in this paper to observe state variables accurately. Moreover, to solve the phase delay problem in active disturbance rejection control (ADRC), Taylor's formula-based tracking differentiator (TTD) is applied in the proposed hybrid control strategy. With appropriate compensate of disturbance, denoted as super-twisting hybrid control, the controlled position signal can follow the reference with small tracking errors, also with improved dynamic performance. Simulation results show that the proposed super-twisting hybrid control has the better anti-disturbance and tracking performance compared with the traditional ADRC. Lastly, semi-physical experimental results further validate the effectiveness of the control strategy for ship-borne PMSMs.

INDEX TERMS Super-twisting extended state observer, Taylor's formula-based tracking differentiator, hybrid control, ship-borne PMSM.

I. INTRODUCTION

PERMANENT magnet synchronous motors (PMSMs) have been developed widely in ship-borne system because of the large torque density, high efficiency and fast response [1]. Considering the disturbances from unknown sea wave fluctuations, it is necessary to enhance the anti-disturbance performance of ship-borne control system. The design specifications of our ship-borne control system are given as follows [2].

(1) Horizontal angle control range: $0° \sim 49°$;
(2) Static error range: $-0.06° \sim 0.06°$;
(3) Dynamic error range: $-0.8° \sim 0.8°$;
(4) The time for angle turns from $0°$ to $49°$: within 8 s.

PID control method is one of the most commonly used control methods in industry. However, the integral part of PID will produce calculation errors, which has restricted limitations when addressing nonlinear problems. Active disturbance rejection control (ADRC) is proposed in [3], which can deal with the nonlinear problem effectively. Therefore, ADRC is widely applied in engineering fields such as photoelectric tracking, artillery control and AC servo system, etc. [4]–[7]. ADRC is comprised of tracking differentiator (TD), extended state observer (ESO) and nonlinear state error feedback (NLSEF). There are numerous adjustable parameters in ADRC, among that phase delay phenomenon is inevitable due to large amount of calculations. To optimize the controller parameters, a novel ADRC based on finite-time convergence extended state observer was presented in [8] to acquire better robustness performance. In order to reduce phase delay, Taylor's formula was utilized to compensate phase delay of differential processing in [9].

The point of improving anti-disturbance performance of ADRC is to improve the estimation accuracy of ESO, a comprehensive summary and systematic analysis on the external disturbance/uncertainty estimation and attenuation methods, for example, disturbance observer based control, ADRC, and composite anti-disturbance control which is given in [10]. Fractional-order extended state observer has been addressed in [11] to affirm the estimated disturbance accurately, but its high-frequency switching gain will cause the chattering phenomenon. Non-singular terminal sliding mode observer was

The review of this article was arranged by Associate Editor Chi-Hua Chen.

proposed to solve the problem of differential state amplify noise and phase delay problems in [12]. A novel finite-time control with time-varying second-order nonlinear disturbance observer is proposed to improve the performance of overcurrent protection and disturbance rejection for PMSM system in [13].

Super-twisting extended state observer (SESO) is widely used in nonlinear systems due to its advantages on convergence speed and anti-disturbance performance [14], [15]. In [16], a third-order super-twisting extended state observer was proved to acquire better dynamic performance in position control loop and more precise disturbance estimation, its stability and convergence speed were also analyzed. A high-order super-twisting extended state observer was proposed in [17], which eliminates the non-derivable term $k_2\text{sign}(e_1)$ in the low-order observer and the second-order sliding surface. Based on above analysis, super-twisting ESO is thereby used to observe disturbances of the studied PMSM system, and then compensated disturbance by NLSEF. In this paper, we proposed a SESO that is able to keep the main above-mentioned advantages of standard super-twisting algorithm.

Super-twisting sliding mode control observer in rotor synchronous frame through integral back stepping is applied in IPMSM [18]. A generalized super-twisting algorithm (GSTA) is proposed in [19], which used to solving the trajectory tracking problem of articulated intervention autonomous underwater vehicle (AIAUVs) in six degrees of freedom (6DOF). Existing modifications of the super-twisting algorithm allow for improved disturbance rejection capability. The properties and design framework of disturbance-tailored super-twisting are analyzed in [20]. The parameters in disturbance-tailored super-twisting controller has been given in [20, eq. (28)]. Chattering phenomenon has been discussed in [21], it has been shown that as the value of the unmodeled dynamic increases the amplitude of chattering increases. The simulation results show that increasing the value of the gain a in super-twisting sliding mode can improve anti-disturbance performance but raises the amplitude of the chattering. Super-twisting sliding mode control (SMC) has been quantized in [22]. With the static uniform quantization strategy, stability properties of the system with quantized state feedback have been obtained. Super-twisting sliding mode control has been compared with conventional sliding mode control [23]. It also point out that reduce chattering amplitude is one of the design difficulty in super-twisting sliding mode control.

The schematic tructure of the proposed super-twisting hybrid control method is given as Fig. 1. In general, working with the PI-based current control and Pulse-Width Modulation (PWM), a super-twisting hybrid control strategy is proposed to stabilize the angle and its speed of PMSM. The measured angle of PMSM is obtained by a resolver, based on which, estimated angle $\hat{\theta}$, angle speed $\hat{\omega}$, disturbance $\hat{d}$ can be given by the super-twisting ESO, and feedback to

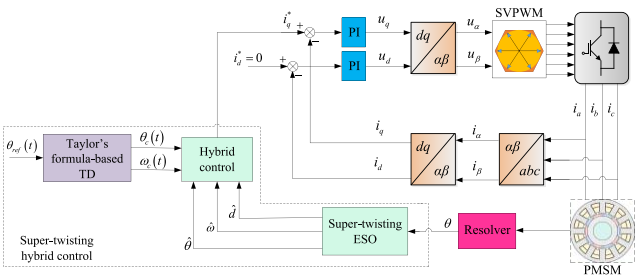

FIGURE 1. Structure of super-twisting hybrid control.

hybrid control. Then, the q-axis current reference i_q^* is given by the hybrid control and feedforward to calculate the i_q tracking error, which can derive the q-axis voltage via a PI controller.

The main contributions of this article are listed as follows.

(1) A novel super-twisting ESO is introduced for ship-borne PMSM hybrid control. Super-twisting algorithm has the merits of finite-time convergence and robustness. Based on the super-twisting ESO, the ship-onboard PMSM system disturbance can be estimated fast. (2) Compared with ADRC, super-twisting hybrid control has fewer parameters to adjust; Moreover, a better dynamic performance can be achieved by the proposed control strategy. (3) Taylor's formula-based TD (TTD) is applied to overcome the phase delay in traditional TD, which improves tracking accuracy effectively.

II. MATHEMATICAL MODEL OF PMSM

There are two PMSMs in this ship-borne control system, one of them is used to control the ship vertical angle, another one is used to control the ship horizontal angle. This paper focuses on the horizontal angle control and the mathematical model of PMSM in d-q axis is given as:

$$\begin{cases} \dot{i}_d = -\frac{R}{L_d} i_d + n\omega i_q + \frac{u_d}{L_d} \\ \dot{i}_q = -\frac{R}{L_q} i_q - n\omega i_d - \frac{n\psi_f}{L_q} + \frac{u_q}{L_q} \\ \dot{\omega} = \frac{1}{J}\left(K_e i_q - T_L - B\omega\right) \end{cases} \tag{1}$$

where u_d, u_q are stator voltages; i_d, i_q are stator currents; L_d, L_q are stator inductances. In surface mounted PMSMs, $L_d = L_q = L$; ψ_f is magnetic flux; R is stator resistance; p is pole-pair numbers of PMSM; J is inertia moment of rotor; B is friction modulus; ω is angular velocity of rotor; K_e is torque constant ($T_e = \frac{3}{2} n\psi_f i_q = K_e i_q$, n is pole-pair number); T_L is load torque.

Assume $i_d = 0$, the mathematical model of PMSM can be rewritten as

$$\begin{cases} \dot{i}_q = -\frac{R}{L} i_q - n\omega i_d - \frac{n\psi_f}{L} + \frac{u_q}{L} \\ \dot{\omega} = \frac{1}{J}\left(K_e i_q - T_L - B\omega\right) \end{cases} \tag{2}$$

Set $b = \frac{K_e}{J}$, $d(t)$ is total disturbance, the mathematical can be simplified as

$$\begin{cases} \dot{\theta} = \omega \\ \dot{\omega} = bi_q^* + d(t) \\ d(t) = -\frac{T_L}{J} - \frac{B\omega}{J} - \frac{K_e}{J}\left(i_q^* - i_q\right) \\ y = \theta. \end{cases} \tag{3}$$

III. SUPER-TWISTING HYBRID CONTROL

A. TAYLOR'S FORMULA-BASED TD

One of the crucial objectives of TD design is to eliminate the phase delay. Since the Taylor's formula can compensate the phase delay effectively [9], it is used in the TD design, as

$$\begin{aligned} \tilde{g}_d(k_{n+1}) = g_d(k_n) &+ \frac{g_d'(k_n)}{1!}(k_{n+1} - k_n) + \frac{g_d''(k_n)}{2!}(k_{n+1} - k_n)^2 \\ &+ \cdots + \frac{g_d^{(n)}(k_n)}{n!}(k_{n+1} - k_n)^n \\ &+ \frac{g_d^{(n+1)}(\xi)}{(n+1)!}(k_{n+1} - k_n)^{n+1} \end{aligned} \tag{4}$$

Traditional Taylor's formula-based TD is

$$\tilde{g}_d(k_{n+1}) = g_d(k_{n+1}) + r_C \Delta k \cdot g_d'(k_{n+1}) \tag{5}$$

where, $\Delta k = k_{n+1} - k_n = r_C h$ is delay time, compensation step is r_C, set $n \le 4$.

According to [5], the nonlinear function $fst(\cdot)$ is given as

$$\begin{aligned} fst(x_1(k), x_2(k), r, h) &= \begin{cases} -r(a/d), & |a| \le d \\ -rsgn(a), & |a| > d \end{cases} \\ a &= \begin{cases} x_2(k) + \frac{a_0 - d}{2} sgn(y(k)), & |y(k)| > d_0 \\ x_2(k) + \frac{y(k)}{h}, & |y(k)| \le d_0 \end{cases} \\ d = rh,\ d_0 = dh,\ a_0 &= \sqrt{d^2 + 8r|y(k)|} \\ y(k) &= x_1(k) + hx_2(k) - y_d(k) \end{aligned} \tag{6}$$

where $y_d(k)$ is reference signal, $h$is step length and r denote speed. $x_1(k)$ and $x_2(k)$ tracking $y_d(k)$ and $\dot{y}_d(k)$ respectively.

Denote θ^* as the tracking reference and Δt as the time interval, the second-order TD is

$$\theta^*(t) = \theta(t) + \theta'(t)\Delta t + \frac{1}{2}\theta''(\xi)\Delta t^2 \tag{7}$$

where $\theta^*(t)$ is the input, $\theta(t + \Delta t)$ is the output. Combined with $fst(\cdot)$ function, Taylor's formula-based TD is finally derived as

$$\begin{aligned} \theta_c(t + \Delta t) &= \theta(t) + \theta'(t)\Delta t + \frac{1}{2}\theta''(\xi)\Delta t^2 \\ \omega_c(t + \Delta t) &= \omega(t) + \Delta t \cdot fst(\theta(k), \omega(k), r_0, h_0) \\ &\quad + \frac{1}{2}\omega''(\xi)\Delta t^2. \end{aligned} \tag{8}$$

B. SUPER-TWISTING EXTENDED STATE OBSERVER

Super-twisting hybrid control method is composed of TTD, hybrid control and super-twisting ESO, which is drawn in the dotted block of Fig. 1. Dotted box in Fig. 1 is enlarged in Fig. 2. TTD transfers differentiator signals to hybrid control while super-twisting ESO transfers the estimate disturbance

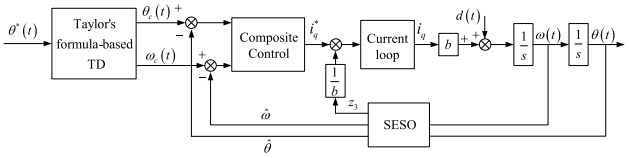

FIGURE 2. Structure of position and speed loop.

$\hat{d}$ to hybrid control, which is then actively compensated. Set state variablesθ, ω and d as state variables, then the state equations are given as

$$\begin{cases} \dot{\theta} = \omega \\ \dot{\omega} = bi_q^* + d \\ y = \theta. \end{cases} \tag{9}$$

1) TRADITIONAL ESO

Traditional ESO is given as:

$$\begin{aligned} e(k) &= z_1(k) - y(k), \\ z_1(k+1) &= z_1(k) - h[z_2(k) - \beta_{01}e(k)], \\ z_2(k+1) &= z_3(k) - h\left[z_3(k) - \beta_{02}fal(e(k), \alpha_1, \delta_1) + bu(k)\right], \\ \dot{z}_3(k+1) &= z_3(k) - h\beta_{03}fal(e(k), \alpha_2, \delta_1). \end{aligned} \tag{10}$$

where, $fal(e(k), \alpha, \delta) = \begin{cases} \frac{e(k)}{\delta^{1-\alpha}} & |e(k)| \le \delta \\ |e(k)|^{\alpha}\text{sign}(e(k)) & |e(k)| > \delta \end{cases}$. It can be known that h, β_{01}, β_{02}, β_{03}, α_1, α_2, δ_1 are all the parameters need to be adjusted.

2) SESO DESIGN

There are many parameters in the traditional ESO that need to adjust, making trail-and-error process complicated. In contrast, super-twisting ESO has better observation accuracy and fewer parameters to adjust. $\hat{\theta}$, $\hat{\omega}$ and $\hat{d}$ represent the observation values of θ, ω and d. Super-twisting ESO can be given as

$$\begin{cases} e_2 = \hat{\omega} - \omega_c \\ \dot{\hat{\theta}} = \hat{\omega} + \beta e_2 \\ \dot{\hat{\omega}} = -k_1\phi_1(\hat{\omega}) + \hat{d} + bi_q^* \\ \dot{\hat{d}} = -k_2\phi_2(\hat{\omega}) + \rho(t) \end{cases} \tag{11}$$

where

$$\begin{cases} \phi_1(\hat{\omega}) = |\hat{\omega}|^{1/2}\text{sign}(e_2) + k_3 e_2 \\ \phi_2(\hat{\omega}) = \phi_1'(\hat{\omega})\phi_1(\hat{\omega}) = \frac{1}{2}\text{sign}(\hat{\omega}) + \frac{3}{2}k_3|\hat{\omega}|^{1/2}\text{sign}(\hat{\omega}) + k_3^2\hat{\omega} \end{cases}$$

The parameters are obtained by setting $k_1 = 6\xi^{1/6}$, $k_2 = 11\xi^{1/2}$ and $k_3 = 6\xi$, where the constant boundary ξ is defined as $|\dot{\hat{d}}| < \xi$ [17]. Sinusoidal disturbance is defined as $\rho(t) = 5\sin(\frac{2\pi}{4.2}t)$ in this paper, $\beta(\beta > 0)$ is the error correction gain, which is set as $\beta = 0.01$ in this paper.

3) STABILITY ANALYSIS

In order to analyses the stability of super-twisting ESO, simplified Lyapunov function is proposed in [24]:

$$V = \varphi^T P \varphi \tag{12}$$

State variable is $\varphi^T = [\phi_1(\hat{\omega}), \hat{d}]$, then the derivative of φ is

$$\dot{\varphi} = \begin{bmatrix} \phi_1'(\hat{\omega})\dot{\hat{\omega}} \\ -k_2\phi_2(\hat{\omega}) + \rho(t) \end{bmatrix} = \phi_1'(\hat{\omega}) \begin{bmatrix} -k_1\phi_1(\hat{\omega}) + \hat{d} + bi_q^* \\ -k_2\phi_1(\hat{\omega}) + \frac{\rho(t)}{\phi_1'(\hat{\omega})} \end{bmatrix} = \phi_1'(\hat{\omega})(A\varphi + BD) \tag{13}$$

where D is disturbance matrix, A and B are coefficient matrix, which are given as

$$A = \begin{bmatrix} -k_1 & 1 \\ -k_2 & 0 \end{bmatrix}, \ B = \begin{bmatrix} b & 0 \\ 0 & \frac{1}{\phi_1'(\hat{\omega})} \end{bmatrix}, \ D = \begin{bmatrix} i_q^* \\ \rho \end{bmatrix}.$$

Assume $P(P = P^T > 0)$ is a symmetric positive definite matrix, and there is a matrix $\Theta = \begin{bmatrix} \theta_1 & 0 \\ 0 & \theta_2 \end{bmatrix}$. $\theta_1, \theta_2, \varepsilon$ are positive constant, there will be a matrix inequality:

$$\begin{bmatrix} A^TP + PA + \varepsilon P + R & PB + S^T \\ B^TP + S & -\Theta \end{bmatrix} \leq 0 \tag{14}$$

According to [20], the convergence time is given as

$$T = \frac{2}{\varepsilon k_3} \ln\left(\frac{2k_3}{\lambda_{\min}^{\frac{1}{2}}\{P\}} V^{\frac{1}{2}}(z_2(0) + 1) \right) \tag{15}$$

The derivative of Lyapunov function is $\dot{V} = \dot{\varphi}^T P\varphi + \varphi^T P\dot{\varphi}$, it can be derived as [25]:

$$\begin{aligned} \dot{V} &= \dot{\varphi}^T P\varphi + \varphi^T P\dot{\varphi} \\ &= \phi_1'(\hat{\omega})\left(\varphi^T AP + d^T B^T P\right)\varphi + \varphi^T P(\phi_1'(\hat{\omega})(A\varphi + BD)) \\ &= \phi_1'(\hat{\omega})\left[\varphi^T\left(A^TP + PA\right)\varphi + D^TB^TP\varphi + \varphi^T PBD\right] \\ &= \phi_1'(\hat{\omega})\begin{bmatrix} \varphi \\ D \end{bmatrix}^T \begin{bmatrix} A^TP + PA & PB \\ B^TP & 0 \end{bmatrix} \begin{bmatrix} \varphi \\ D \end{bmatrix} \\ &\leq \phi_1'(\hat{\omega})\begin{bmatrix} \varphi \\ D \end{bmatrix}^T \begin{bmatrix} A^TP + PA & PB \\ B^TP & -\Theta \end{bmatrix} \begin{bmatrix} \varphi \\ D \end{bmatrix} \\ &\leq -\phi_1'(\hat{\omega})\varepsilon V = -\frac{1}{2|\hat{\omega}|^{\frac{1}{2}}}\varepsilon V - k_3\varepsilon V \\ &\leq -\frac{\varepsilon\lambda_{\min}^{\frac{1}{2}}\{P\}}{2} V^{\frac{1}{2}} - k_3\varepsilon V \leq 0. \end{aligned} \tag{16}$$

This proves that the system can converge to the origin point in finite time.

C. FINITE TIME CONTROL

Finite time control is a novel control method, which can converge to origin point within finite time, the control law is:

$$u = -k'\text{sign}(e)|e|^{\alpha}. \tag{17}$$

Finite time control is combined with super-twisting ESO in this paper, which is given as

$$i_q^* = \frac{1}{b}\left[-k'\text{sign}(e_2)|e_2|^{\alpha} - z_3\right] \tag{18}$$

where k' is proportion gain, $0 < \alpha < 1$.

TABLE 1. Parameters in simulation and experiment.

Symbol	Parameter	Value
J	moment of inertia	$5.556\times10^{-3}\text{kg}\times\text{m}^2$
B	friction coefficient	$1.43\times10^{-4}(\text{N}\times\text{m})/(\text{rad}\times\text{s}^{-1})$
T_L	disturbing moment	$9.32\times10^{3}\text{kg}\times\text{m}^2$
K_t	motor torque factor	$0.175(\text{N}\times\text{m})/\text{A}$
i	reduction ratio	1039
$L_d = L_q$	stator inductance	21.24mH
p	pole pairs	3
ψ_f	motor magnetic flux	0.65Wb
k_1	Parameter in SESO	6.036
k_2	Parameter in SESO	163.156
k_3	Parameter in SESO	1320
β	Parameter in SESO	0.01

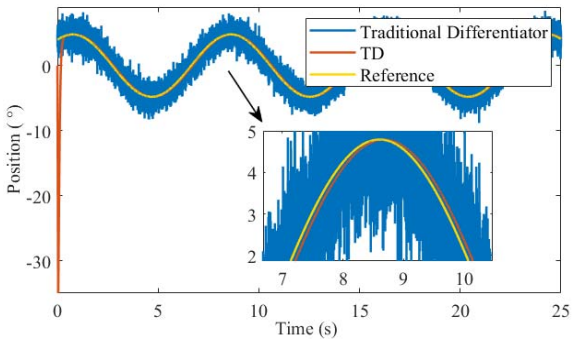

FIGURE 3. Differentiator with random noise.

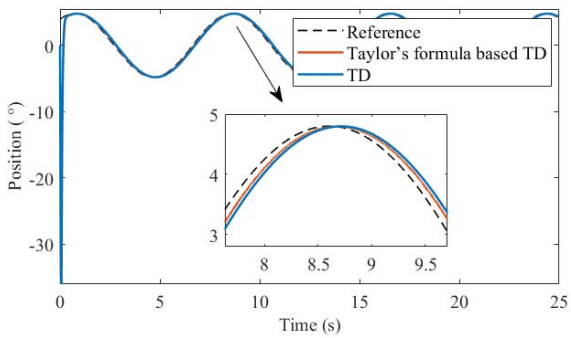

FIGURE 4. Differentiator tracking curve.

IV. SIMULATION RESULTS

In order to test the performance of super-twisting hybrid control, stepped and sinusoidal signal tracking simulations are conducted in MATLAB/Simulink. Parameters in Taylor's formula-based TD are set as $h = 0.01$, $r_C = 1000$. The parameters of PMSM are listed in Table 1.

Differentiator simulation results are given by Figs. 3 & 4. In the processing of traditional differentiator, noise is usually amplified.

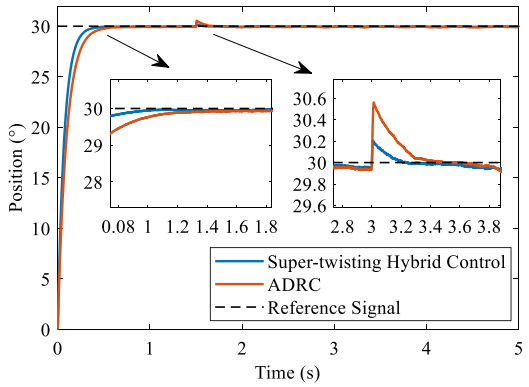

FIGURE 5. Response with step disturbance.

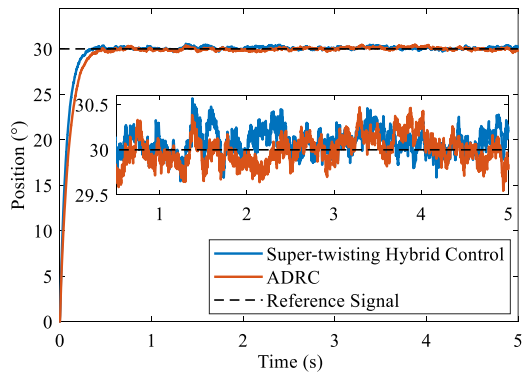

FIGURE 6. Step simulation with random disturbances.

TABLE 2. Performance comparison of step response.

Control Method	Convergence Time (s)	Recover Time (s)	RMSE
Super-twisting Hybrid Control	1.07	0.2	2.5942
ADRC	1.39	0.4	2.9829

In Fig. 3, the maximum ripple of traditional differentiator is about 7.39°, while TD is 0.003° TD. It shows TD can suppress noise effectively. The maximum ripple of traditional differentiator is about 7.39°, while TD is 0.003°. Furthermore, as shown in Fig. 4, as the same position, compared with reference signal, TD has delayed 0.036s, while Taylor's formula based TD delayed 0.03s. Therefore, compared with traditional TD, Taylor's formula-based TD can track the reference signal more accurately.

In order to validate the anti-disturbance of the proposed method, two different forms of external disturbances are loaded in simulations. In this section, step disturbance and random disturbances is applied in simulation, the experimental results are given in Fig. 5 and Fig. 6 respectively.

Step response simulation is conducted with step disturbance and random disturbances, as shown in Figs. 5&6 respectively. It can be seen from Fig. 5 and summarized in Table 2 that, super-twisting hybrid control can reach 30° within 1.07s, while ADRC needs 1.39s to reach the reference angle. Super-twisting hybrid control can give

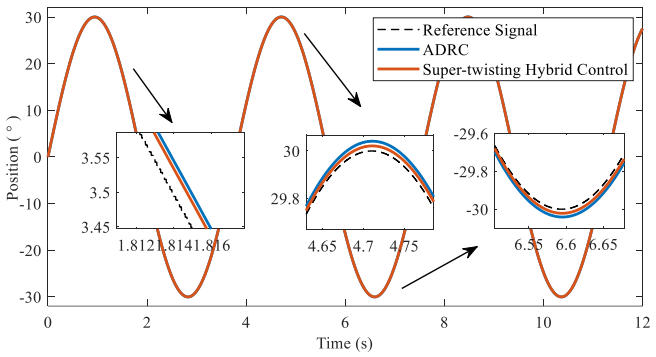

FIGURE 7. Sinusoidal tracking simulation.

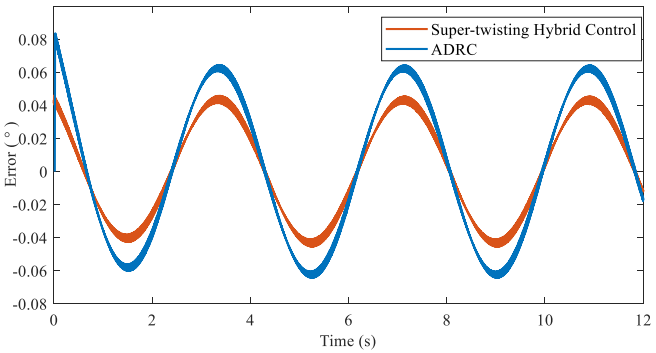

FIGURE 8. Sinusoidal tracking error.

a better anti-disturbance performance, which takes 0.2s to recover, while ADRC needs 0.4s. This experiment proved super-twisting hybrid control has fast convergence speed and better anti-disturbance.

In this case of loading random disturbance, whose noise amplitude is about 3.6 degree, tracking curves are shown in Fig. 6. It can be seen that super-twisting hybrid control has high level chattering compared with ADRC after 1.5s, but RMSE is relatively lower (given in Table 2). This simulation result demonstrates the proposed super-twisting hybrid control has better anti-disturbance performance than ADRC, but chattering phenomenon needs to be solved.

Chattering phenomenon is mainly caused by unmolded dynamics and high feedback gain or discontinuous control. Super-twisting algorithm has the merit of finite time convergence, which implies a non-Lipschitzian switching function with infinite derivative in the origin, it will result in high amplitude chattering problem [23]. It can be seen from Fig. 6, compared to ADRC, the chattering suppression and theoretical analysis for super-twisting hybrid control faces great difficulties for quite some time. This experimental result shows the design difficulty of super-twisting control is how to balance the conflicts between chattering suppression and finite time convergence.

The comparative simulation results of ADRC and super-twisting hybrid control for sinusoidal signal tracking are shown in Figs. 7 & 8. In this simulation, the sinusoidal signal's amplitude is 30° with period of 3.768s. It can be

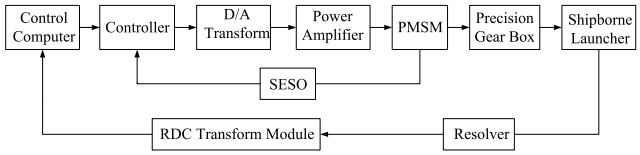

FIGURE 9. Structure of shipborne rocket launcher servo system.

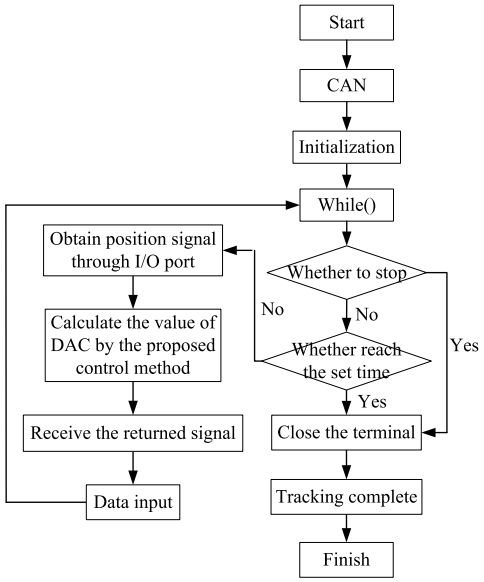

FIGURE 10. Implementation flowchart of driving PMSM.

seen from Fig.7 that, compared with ADRC, super-twisting hybrid control has a smaller phase delay. The corresponding sinusoidal signal tracking error of the two controllers are shown in Fig. 8. In the steady state, the maximum error of super-twisting hybrid control is only 0.045° while ADRC is 0.064°. The tracking error of super-twisting hybrid control is smaller than ADRC, which demonstrates super-twisting hybrid control has a higher dynamic tracking accuracy.

V. SEMI-PHYSICAL EXPERIMENT

The overall structure of shipborne rocket launcher system is shown in Fig. 9, where STM32 micro-controller uses C programming language to simulate the position loop and speed loop control. Control computer is used to send command signal through C++ programming language.

We use Visual C++6.0 (VC) as the development platform. The test uses an embedded computer to simulate the state of the fire control computer and send signals to the system through Controller Area Network (CAN). After initializing the chip, the system enters the cycle program and waits for the generation of the corresponding interrupt, then executes the service program of the corresponding interrupt. The implementation flow chart for driving PMSM is shown in Figure 10.

The proposed super-twisting hybrid control is applied to the position loop of the ship-borne PMSM and tested on a semi-physical experiment rig. Step response and

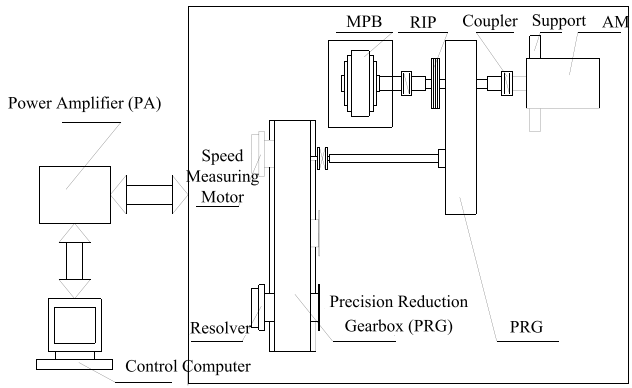

(a) Schematic diagram of the semi-physical experiment rig

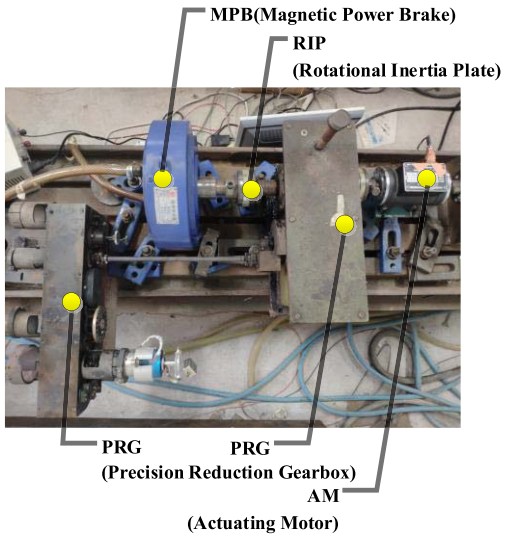

(b) Photo of the semi-physical experiment rig

FIGURE 11. Semi-physical experiment platform.

sinusoidal signal tracking experiments are conducted on the semi-physical platform which is shown in Fig. 11.

Firstly, as shown in Fig. 11(a), input reference signals to the servo system via control computer and the connected power amplifier (AP). Secondly, adjust the load position through precision reduction gearbox (PRG). Lastly, position and velocity signals are measured by speed measuring motor and resolver, then processed by the proposed controller to control servo system. For the practical ship onboard application, magnetic power brake (MPB) is used to simulate friction torque and rotational inertia plate (RIP) is used to simulate moment of inertia in the system. Actuating motor (AM) is the studied PMSM. Fig. 11(b) shows the photo of semi-physical experiment rig.

Step response experiment is conducted to validate the response speed of super-twisting hybrid control method while the tracking sinusoidal signal is used to demonstrate the dynamic performance, whose amplitude is 30° and the period is 4.2s.

All the experimental results are given in Figs. 12-14. It can be seen from Fig. 12 that the proposed control method

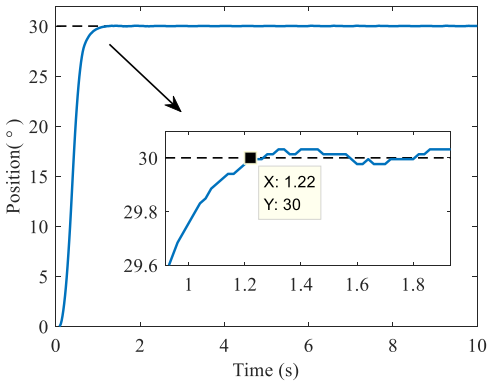

FIGURE 12. Semi-physical platform structure.

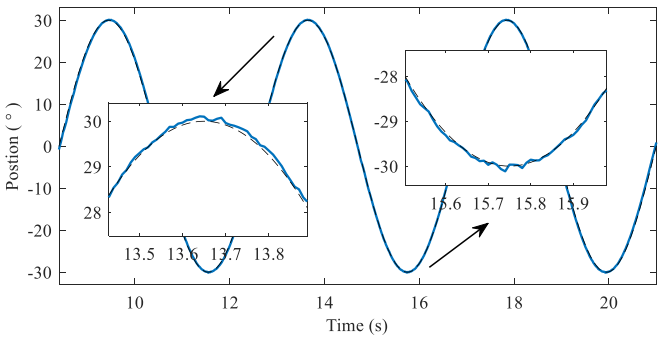

FIGURE 13. Semi-physical sinusoidal signal tracking.

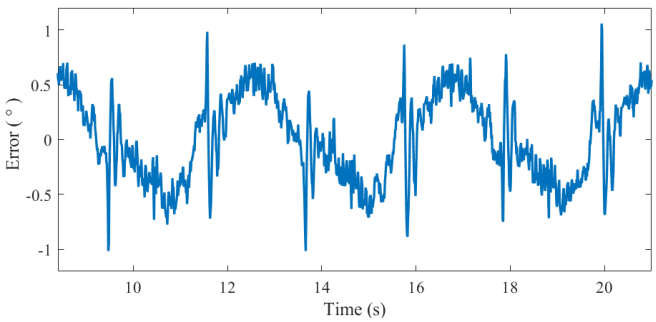

FIGURE 14. Semi-physical sinusoidal signal tracking error.

can reach the reference angle within 1.22s. The steady-state error of this system is around 0.027°, which meets the design requirement of steady-state error, i.e., less than 0.06° (0.2% of reference signal).

Sinusoidal signal tracking curve is shown as Fig. 13 and the corresponding tracking error is drawn as Fig. 14. The maximum absolute tracking error is approximately 0.62° and the maximum step value is 0.98°. All these results are acceptable for the practical PMSM applications onboard ships.

VI. CONCLUSION

A novel anti-disturbance technique for ship-borne PMSM is presented in this paper. The main issue of ship-borne controller design is to improve anti-disturbance performance.

By introducing Taylor's formula-based TD to the super-twisting ESO, the position signal can be controlled to follow the given reference within a finite time. From the simulation results, it can be concluded that super-twisting hybrid control has faster response and better dynamic performance compared with ADRC. In addition, the experimental results further validate the proposed control method on a semi-physical PMSM platform.

The finite-time convergence and robustness of STA have been proved by geometrical methods in [26]. It's interesting that finite time convergence is in conflict with chattering suppression problem. Super-twisting method may cause a larger chattering problem which is shown in Fig. 6. This design difficulty needs to be solved in future work. Chattering phenomenon is mainly caused by unmolded dynamics. The problems of model uncertainties and input nonlinearities are also commonly seen in real PMSM system, and adaptive or fuzzy structures or NNs may also provide effective solutions to handle them in future work [13], [27], [28]. In addition, the effects of main design parameters on the system performance can be further investigated.

REFERENCES

[1] Y.-J. Wu and G.-F. Li, "Adaptive disturbance compensation finite control set optimal control for PMSM systems based on sliding mode extended state observer," *Mech. Syst. Signal Process.*, vol. 98, pp. 402–414, Jan. 2018.

[2] R. Wang, B. Lu, R. Hou, and Q. Gao, "FOPID improved ADRC in AC servo systems," *China Mech. Eng.*, vol. 30, no. 16, pp. 1989–1995, 2019.

[3] J. Han, "From PID to active disturbance rejection control," *IEEE Trans. Ind. Electron.*, vol. 56, no. 3, pp. 900–906, Mar. 2009.

[4] M. Lv, R. Hou, Y. Ke, and Y. Hou, "Compensation method for miss distance time-delay of electro-optical tracking platform," *J. Xi'an Jiaotong Univ.*, vol. 53, no. 11, pp. 141–147, 2019.

[5] Q. Gao, Z. Sun, G. Yang, R. Hou, L. Wang, and Y. Hou, "A novel active disturbance rejection-based control strategy for a gun control system," *J. Mech. Sci. Technol.*, vol. 26, no. 12, pp. 4141–4148, 2012.

[6] C. Liu, G. Luo, W. Tu, and H. Wan, "Servo systems with double closed-loops based on active disturbance rejection controllers," *Proc. Chin. Soc. Elect. Eng.*, vol. 37, no. 23, pp. 7032–7039, 2017.

[7] M. Ran, Q. Wang, and C. Dong, "Active disturbance rejection control for uncertain nonaffine-in-control nonlinear systems," *IEEE Trans. Autom. Control*, vol. 62, no. 11, pp. 5830–5836, Nov. 2017.

[8] Z. Cai, J. Lou, J. Zhao, K. Wu, N. Liu, and Y. X. Wang, "Quadrotor trajectory tracking and obstacle avoidance by chaotic grey wolf optimization-based active disturbance rejection control," *Mech. Syst. Signal Process.*, vol. 128, pp. 636–654, Aug. 2019.

[9] J. Feng, W. Wang, and Y. Chen, "An improved tracking-differentiator filter based on Taylor's formula," *Optik Int. J. Light Electron Opt.*, vol. 158, pp. 1026–1033, Apr. 2018.

[10] W.-H. Chen J. Yang, L. Guo, and S. Li, "Disturbance-observer-based control and related methods—An overview," *IEEE Trans. Ind. Electron.*, vol. 63, no. 2, pp. 1083–1095, Feb. 2016.

[11] J. Huang, P. Ma, G. Bao, F. Gao, and X. Shi, "Research on position servo system based on fractional-order extended state observer," *IEEE Access*, vol. 8, pp. 102748–102756, 2020.

[12] X. J. Chang, B. Peng, L. Liu, and L. Gao, "A novel nonsingular terminal sliding mode observer for sensorless control of permanent magnet synchronous motor," *J. Xi'an Jiaotong Univ.*, vol. 50, no. 1, pp. 85–99, 2016.

[13] Y. Wang, H. Yu, and Y. L. Liu, "Speed-current single-loop control with overcurrent protection for PMSM based on time-varying nonlinear disturbance observer," *IEEE Trans. Ind. Electron.*, vol. 69, no. 1, pp. 179–189, Jan. 2022.

[14] L. Zhao, C. Zheng, Y. Wang, and B. Liu, "A finite-time control for a pneumatic cylinder servo system based on a super-twisting extended state observer," *IEEE Trans. Syst., Man, Cybern., Syst.*, vol. 51, no. 2, pp. 1164–1173, Feb. 2021.

[15] D. Wang *et al.*, "Rotor position estimation method for permanent magnet synchronous motor based on super-twisting sliding mode observer," in *Proc. Chin. Control Conf.*, Wuhan, China, 2018, pp. 5634–5638.

[16] T. Zhang, Z. Xu, J. Li, H. Zhang, and C. Gerada, "A third-order super-twisting extended state observer for dynamic performance enhancement of sensorless IPMSM drives," *IEEE Trans. Ind. Electron.*, vol. 67, no. 7, pp. 5948–5958, Jul. 2020.

[17] A. Chalanga, S. Kamal, L. Fridman, B. Bandyopadhyay, and J. A. Moreno, "Implementation of super-twisting control: Super-twisting and higher order sliding-mode observer-based approaches," *IEEE Trans. Ind. Electron.*, vol. 63, no. 6, pp. 3677–3685, Jun. 2016.

[18] W. A. Teklu and X. Ge, "Speed sensorless control of IPMSM using super-twisted sliding mode observer based integral backstepping theory," in *Proc. IEEE Int. Power Electron. Appl. Conf. Exposit. (PEAC)*, Shenzhen, China, 2018, pp. 1–6, doi: 10.1109/PEAC.2018.8590425.

[19] I.-L. G. Borlaug, K. Y. Pettersen, and J. T. Gravdahl, "Tracking control of an articulated intervention autonomous underwater vehicle in 6DOF using generalized super-twisting: Theory and experiments," *IEEE Trans. Control Syst. Technol.*, vol. 29, no. 1, pp. 353–369, Jan. 2021, doi: 10.1109/TCST.2020.2977302.

[20] H. Haimovich and H. De Battista, "Disturbance-tailored super-twisting algorithms: Properties and design framework," *Automatica*, vol. 101, pp. 318–329, Mar. 2019.

[21] A. Swikir and V. Utkin, "Chattering analysis of conventional and super twisting sliding mode control algorithm," in *Proc. 14th Int. Workshop Variable Struct. Syst. (VSS)*, Nanjing, China, 2016, pp. 98–102, doi: 10.1109/VSS.2016.7506898.

[22] Y. Yan, S. Yu, and X. Yu, "Quantized super-twisting algorithm based sliding mode control," *Automatica*, vol. 105, pp. 43–48, Jul. 2019.

[23] V. Utkin, "Discussion aspects of high-order sliding mode control," *IEEE Trans. Autom. Control*, vol. 61, no. 3, pp. 829–833, Mar. 2016, doi: 10.1109/TAC.2015.2450571.

[24] J. A. Moreno and M. Osorio, "A Lyapunov approach to second-order sliding mode controllers and observers," in *Proc. 47th IEEE Conf. Decis. Control (CDC)*, 2008, pp. 2856–2861.

[25] J. A. Moreno, "A linear framework for the robust stability analysis of a generalized super-twisting algorithm," in *Proc. Int. Conf. Elect. Eng. Comput. Sci. Autom. Control (CCE)*, 2010, pp. 1–6.

[26] A. Levant, "Principles of 2-sliding mode design," *Automatica*, vol. 43, no. 4, pp. 576–586, Apr. 2007.

[27] T. Yang, N. Sun, Y. Fang, X. Xin, and H. Chen, "New adaptive control methods for *n*-link robot manipulators with online gravity compensation: Design and experiments," *IEEE Trans. Ind. Electron.*, vol. 69, no. 1, pp. 539–548, Jan. 2022, doi: 10.1109/TIE.2021.3050371.

[28] T. Yang, N. Sun, and Y. Fang, "Adaptive fuzzy control for a class of MIMO underactuated systems with plant uncertainties and actuator deadzones: Design and experiments," *IEEE Trans. Cybern.*, early access, Feb. 2, 2021, doi: 10.1109/TCYB.2021.3050475.